

IN THE UNITED STATES PATENT AND TRADEMARK OFFICE

In re application of:

Larry C. Olsen et al.

Application No. 10/726,744

Filed: December 2, 2003

Confirmation No. 6833

For: THERMOELECTRIC DEVICES AND
APPLICATIONS FOR THE SAME

Examiner: Jeffrey Thomas Barton

Art Unit: 1795

Attorney Reference No. 23-65037-01

FILED VIA EFS

ON 4/7/09

FILED VIA ELECTRONIC FILING SYSTEM
COMMISSIONER FOR PATENTS

SUPPLEMENTAL AMENDMENT

This Amendment is filed in response to the telephone interview of February 12, 2009.
Please amend the referenced application as follows:

Amendments to the Claims are reflected in the listing of claims, which begins on
page 2.

Remarks begin on page 7.

Claims

1. (Currently amended) A thermoelectric power source comprising:
a flexible substrate having an upper surface; and
a plurality of thermoelectric couples with the thermoelectric couples comprising:
(a) a sputter deposited thin film p-type thermoelement positioned on the upper surface of the flexible substrate;
(b) a sputter deposited thin film n-type thermoelement positioned on the upper surface of the flexible substrate adjacent the p-type thermoelement;
(c) an electrically conductive member positioned on the flexible substrate, and electrically connecting the first end of the p-type thermoelement with the second end of the n-type thermoelement, wherein the p-type or the n-type thermoelements comprise Bi_xTe_y , Sb_xTe_y , or Bi_xSe_y wherein x and y form greater than in incidental amount of a non-stoichiometric compound and x is about 2 and y is about 3; and
wherein the thermoelectric couples are formed on a single substrate and the flexible substrate is in a coil configuration or an accordion configuration.

2. (Currently amended) A thermoelectric power source comprising:
a flexible substrate having an upper surface; and
a plurality of thermoelectric couples with the thermoelectric couples comprising:
(a) a sputter deposited thin film p-type thermoelement positioned on the upper surface of the flexible substrate;
(b) a sputter deposited thin film n-type thermoelement positioned on the upper surface of the flexible substrate adjacent the p-type thermoelement;
(c) an electrically conductive member positioned on the flexible substrate, and electrically connecting the first end of the p-type thermoelement with the second end of the n-type thermoelement, wherein the p-type or the n-type thermoelements comprise Bi_xTe_y , Sb_xTe_y , or Bi_xSe_y wherein x is about 2 and y is about 3;
wherein the thermoelectric couples are formed on a single substrate and the flexible substrate is in a coil configuration or an accordion configuration; and
wherein the p-type or the n-type thermoelements have L/A ratios ~~greater than~~ from about 500 cm^{-1} to about $10,000\text{ cm}^{-1}$.

3. (Original) The thermoelectric power source of claim 1 wherein the p-type or the n-type thermoelements have L/A ratios greater than about 1000 cm^{-1} .

4. (Canceled)

5. (Previously presented) The thermoelectric power source of claim 1 wherein the thermoelectric power source has a power output of at least about $1 \text{ }\mu\text{W}$ with a voltage of at least about 0.25 volt.

6. (Previously presented) The thermoelectric power source of claim 1 further comprising at least about 50 thermoelectric couples, wherein the thermoelectric power source has a power output of at least about $1 \text{ }\mu\text{W}$ with a voltage of at least about 0.25 volt.

7. (Original) The thermoelectric power source of claim 6 wherein the p-type or the n-type thermoelements are at least about 1 mm in length and at least about 0.1 mm in width.

8. (Original) The thermoelectric power source of claim 6 wherein the p-type or the n-type thermoelements are at least about 20 angstroms in thickness.

9. (Original) The thermoelectric power source of claim 1 further comprising at least about 1000 thermoelectric couples, wherein the thermoelectric power source has a power output of about 1W with a voltage of at least about 1 volt.

10. (Previously presented) The thermoelectric power source of claim 1 wherein the p-type thermoelements each have a first width, the n-type thermoelements each have a second width, and the first width is different from the second width.

11. (Original) The thermoelectric power source of claim 1 wherein two or more p-type thermoelements are positioned and electrically connected in parallel with one another and the

parallel positioned p-type thermoelements are electrically connected in series to n-type thermoelements.

12. (Previously presented) The thermoelectric power source of claim 1 wherein the thin film p-type thermoelement and/or the thin film n-type thermoelement are co-sputter deposited thin films comprising Bi_xTe_y , Sb_xTe_y , or Bi_xSe_y wherein x is about 2 and y is about 3.

13. (Original) The thermoelectric power source of claim 1 wherein the volume of the thermoelectric power source is less than about 10 cm^3 and has a power output of from about $1 \mu\text{W}$ to about 1 W.

14. (Original) The thermoelectric power source of claim 1 wherein the volume of the thermoelectric power source is less than about 10 cm^3 and provides voltages of greater than about 1 volt.

15. (Original) The thermoelectric power source of claim 14 wherein the thermoelectric power source produces power at temperature differences of about 20°C or less.

16. (Original) The thermoelectric power source of claim 1 wherein two or more n-type thermoelements are positioned and electrically connected in parallel with one another and the parallel positioned n-type thermoelements are electrically connected in series to p-type thermoelements.

17. (Original) The thermoelectric power source of claim 1 wherein the n-type thermoelements are substantially free of selenium.

18. (Original) The thermoelectric power source of claim 1 wherein the flexible substrate is a polyimide.

Claims 19 – 22 (Canceled)

23. (Previously presented) A thermoelectric power source comprising:
multiple thermocouples electrically connected to one another on an upper surface of a single flexible substrate, the thermocouples comprising:
sputter deposited thin film p-type thermoelements having thicknesses of 0.1 mm or greater;
sputter deposited thin film n-type thermoelements alternatingly positioned adjacent the p-type thermoelements, the n-type thermoelements having a thickness of about 0.1 mm or greater;
wherein the thermoelectric power source has a volume of less than about 10 cm^3 and has a power output of from about $1\text{ }\mu\text{W}$ to about 1 W generated by the thermocouples on the single flexible substrate; and
wherein the p-type thermoelements or the n-type thermoelements comprise a Bi_xTe_y , Sb_xTe_y , or Bi_xSe_y alloy where x is about 2 and y is about 3.

24. (Previously presented) The thermoelectric device of claim 23 wherein said multiple thermocouples electrically connected to one another are in series-parallel.

25. (Previously presented) The thermoelectric power source of claim 23 wherein the p-type thermoelements have L/A ratios greater than about 500 cm^{-1} .

Claims 26 – 36 (Canceled)

37. (Currently amended) A thermoelectric power source comprising:
a flexible substrate having an upper surface; and
a thermoelectric couple comprising:
(a) co-sputter deposited alternating thin film p-type and n-type thermoelements positioned on the upper surface of the flexible substrate;
(b) an electrically conductive member positioned on the flexible substrate, and electrically connecting a first end of the p-type thermoelement with a second end of the n-type thermoelement, ~~wherein the p-type or the n-type thermoelements comprise Bi_xTe_y where x is~~

about 2 and y is about 3 wherein the p-type or the n-type thermoelements comprise Sb_xTe_y or Bi_xSe_y wherein x is about 2 and y is about 3; and

(c) wherein the flexible substrate is in a coil configuration.

38. (Previously presented) The thermoelectric power source of claim 37 wherein the p-type thermoelements or the n-type thermoelements are at least about 1 mm in length and at least about 0.1 mm in width.

39. (Previously presented) The thermoelectric power source of claim 37 wherein the volume of the thermoelectric power source is less than about 10 cm^3 and has a power output of from about $1\mu\text{W}$ to about 1 W.

REMARKS

Claims 1-3, 5-18, 23-25 and 37-39 are pending in the present application.

Reconsideration is respectfully requested.

1. Claims 23 and 24 are rejected under 35 U.S.C. §102(b) as allegedly being anticipated by DE 297 23 309 U1 (DE '309).

No anticipation due to missing element in DE'309: Applicants discussed this rejection with the Examiner during the February 12, 2009 interview and it was agreed that with the amendment of claims 23 and 24 to make it even clearer that the recited power output is generated by those thermocouples formed on the single substrate this rejection is now moot.

No obviousness due to missing element in DE'309: Also as discussed, DE'309 does not suggest use of a single substrate and in fact teaches away from use of a single substrate, asserting that coiling or folding the substrate is damaging (see our discussions on this issue in prior Responses, e.g., Amendment filed November 27, 2007, at p. 8, and the Amendment filed May 20, 2008, at p. 6). As discussed throughout the DE'309 reference, polyimide films are used to increase the density of the device by stacking multiple films. (DE'309 English translation, p. 2. Para. 2.)

2. Claims 1-3, 5-10, 12-15, 17, 18, 23-25 and 37-39 are rejected under §103(a) as allegedly being obvious in view of the combination of Migowski (WO 89/07836) and Buist (4,859,250).

Applicants traverse these rejections for at least the reasons below.

Claim 1 has been further amended to recite not just a thermoelectric power source comprising a plurality of thermoelectric couples comprising p-type and n-type thermoelements, wherein the p-type or the n-type thermoelements comprise Bi_xTe_y , Sb_xTe_y , or Bi_xSe_y wherein x and y form a non-stoichiometric compound and x is about 2 and y is about 3, but also to recite that the non-stoichiometric compound is present in greater than an incidental amount.¹

¹ The Examiner will recall that during the interview of February 12, 2009, the Examiner commented that all compounds, although primarily or virtually completely stoichiometric, may contain a trace or incidental amount of non-stoichiometry due to imperfections in the crystallization structure.

Support for the most recent amendment is inherent in the disclosure. Specifically, in several places in the specification Applicant discusses the co-sputtering or simultaneous sputter deposition from two different targets, such as at p. 10, lines 6-10; p. 12, line 28 – p. 13, line 5; Fig. 11 and Examples 1 and 2. Co-sputtering necessarily results in a compound that is primarily non-stoichiometric.

As can readily be seen by reviewing the attached articles, with the co-sputtering deposition process at substrate temperatures and other sputtering parameters as disclosed in the present application, a primarily or completely non-stoichiometric thin film compound will be formed. (See C W Sun et al., Crystallization Behavior of Non-Stoichiometric Ge–Bi–Te Ternary Phase Change Materials for PRAM Application, *J. Phys.: Condens. Matter*, 19 446004 (2007); and Dong-Ho Kim, Eungsun Byon, Gun-Hwan Lee and Sunglae Cho, Effect of deposition temperature on the structural and thermoelectric properties of bismuth telluride thin films grown by co-sputtering, *Thin Solid Films*, Vol. 510, Issues 1-2, 3, Pp. 148-153 (July 2006).)

As stated in Applicant's specification, the non-stoichiometric composition of the p-type and n-type thermoelements is obtained by the disclosed co-sputtering methods (simultaneous sputter deposition using two or more targets), which are non-equilibrium processes (see, e.g., p. 12, lines 28-30). Changing parameters and conditions, including the chamber pressure, the substrate temperature, the deposition rate, the power supplied to the targets, and the reactive gas pressure during the co-sputtering of target materials provides the recited non-stoichiometric Bi_xTe_y , Sb_xTe_y , or Bi_xSe_y compositions. Variation of these parameters allows the fabrication of the recited thermoelements having desirable thermoelectric, electric and thermal properties – that is, the non-stoichiometric co-deposits provide thermoelectric power that greatly exceeds that of purely stoichiometric deposits. FIG. 11 illustrates how the electrical conductivity and the Seebeck coefficient vary as the Bi_xTe_y and Sb_xTe_y compositions change.

Migowski neither teaches nor suggests p-type or the n-type thermoelements comprising Bi_xTe_y , Sb_xTe_y , or Bi_xSe_y wherein x and y form a non-stoichiometric compound and x is about 2 and y is about 3. Buist, cited by the Examiner as making up for the deficiencies of Migowski, also fails to teach or suggest p-type or the n-type thermoelements comprising Bi_xTe_y , Sb_xTe_y , or Bi_xSe_y wherein x and y form a non-stoichiometric compound and x is about 2 and y is about 3.

Even if, *arguendo*, a contention that Buist discloses thermoelements comprising Bi_xTe_y , Sb_xTe_y , or Bi_xSe_y wherein x and y form a non-stoichiometric compounds, as recited in amended

claim 1 (which it does not) was taken as correct, Buist fails to act as prior art for such a contention because Buist does not enable the making of such thermoelement compositions.

There is no anticipation or prima facie obviousness if there is not also enablement of that for which the art is cited.

"In determining that quantum of prior art disclosure which is necessary to declare an applicant's invention 'not novel' or 'anticipated' within section 102, the stated test is whether a reference contains an 'enabling disclosure'... ." *In re Hoeksema*, 399 F.2d 269, 158 USPQ 596 (CCPA 1968). The disclosure in an assertedly anticipating reference must provide an enabling disclosure of the desired subject matter; mere naming or description of the subject matter is insufficient, if it cannot be produced without undue experimentation. *Elan Pharm., Inc. v. Mayo Found. For Med. Educ. & Research*, 346 F.3d 1051, 1054, 68 USPQ2d 1373, 1376 (Fed. Cir. 2003).

Accordingly, claim 1 is allowable over the art of record and withdrawal of the rejection is respectfully requested.

Claim 2 as previously amended recites, in part, a thermoelectric power source comprising, in part, sputter deposited thin film p-type and n-type thermoelements, wherein the p-type or the n-type thermoelements have L/A ratios from about 500 cm^{-1} to about $10,000 \text{ cm}^{-1}$. (Support for this amendment is in the specification at, e.g., p. 4, lines 1-3 and 15-16.) Neither Migowski nor Buist teach or suggest such an L/A ratio.

The L/A ratios are critical parameters of the claimed devices and such criticality is disclosed in the present application. Please see the § 1.132 Declaration of John DeSteele supporting this statement. Neither Migowski nor Buist nor any other reference of record, teach or suggest such L/A ratios or even recognize the importance of such a ratio and as such, claim 2 is not obvious and is allowable over the art of record.

Claims 3, 5-10, 12-15, and 17-18 are allowable for at least the same reasons as set forth in regard to claims 1 and 2.

Claim 23-25 as previously amended recite, in part, a thermoelectric power source comprising multiple thermocouples electrically connected to one another; the thermocouples comprising sputter deposited thin film p-type and n-type thermoelements having thicknesses of about 0.1 mm or greater. As noted by the Examiner, Migowski discloses much thinner (by orders of magnitude) thermoelements (p. 4, layer thickness of 0.005 mm) and asserts that the layers be as thin as possible. Buist does not disclose a layer thickness at all – completely failing to recognize the importance of this parameter. Furthermore, neither reference teaches or

suggests how to achieve such thicknesses – prior art must be enabling to be considered to teach or suggest a feature.

The thicknesses of the thermoelement as recited in the presently claimed device is critical to the operation of the device as the thermoelement thickness, along with other parameters of the thermoelement, determines the ultimate TE power source output. Please see the § 1.132

Declaration of John DeSteele supporting this statement.

Accordingly, claims 23-25 are allowable over the art of record.

Claims 37-39 are herein amended to recite the p-type or the n-type thermoelements comprise Sb_xTe_y or Bi_xSe_y wherein x is about 2 and y is about 3. Nothing in Migowski or Buist teach or suggest Sb_xTe_y or Bi_xSe_y thermoelements.

Claim 38 recites the thermoelectric power source of claim 37 wherein the p-type thermoelements or the n-type thermoelements are at least about 1 mm in length and at least about 0.1 mm in width. Neither Buist nor Migowski teach or suggest such dimensioned thermoelements. The Examiner asserts that such dimensions are merely a design choice – this contention is incorrect. Such dimensions are critical as stated in the § 1.132 Declaration of John DeSteele.

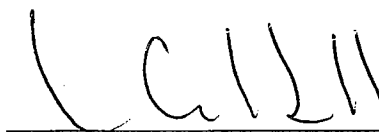
Conclusion

The Examiner is requested to please review the additional arguments set forth in the prior Amendment filed on January 2, 2009 as certain arguments were not re-iterated herein but may not yet have been reviewed by the Examiner.

Respectfully submitted,

KLARQUIST SPARKMAN, LLP

By



Lisa M. Caldwell
Registration No. 41,653

One World Trade Center, Suite 1600
121 S.W. Salmon Street
Portland, Oregon 97204
Telephone: (503) 595-5300
Facsimile: (503) 595-5301

Crystallization behavior of non-stoichiometric Ge–Bi–Te ternary phase change materials for PRAM application

C W Sun¹, M S Youm² and Y T Kim²

¹ Department of Materials Science and Engineering, Korea Advanced Institute of Science and Technology, Daejeon 305-701, Korea

² Semiconductor Materials and Devices Laboratory, Korea Institute of Science and Technology, Seoul 136-791, Korea

E-mail: suxxus@kaist.ac.kr

Received 21 June 2007, in final form 9 August 2007

Published 24 September 2007

Online at stacks.iop.org/JPhysCM/19/446004

Abstract

We investigated the properties of a Ge–Bi–Te ternary chalcogenide thin film which was deposited on a SiO₂/Si substrate by varying RF-sputtering power on the GeTe and Bi target. The aim was to search for an appropriate candidate for a new phase change memory. Various analyses are conducted in order to investigate the composition, phase separation, and crystallization behavior of the Ge–Bi–Te alloy. The XRD results of each annealed sample showed that the Ge–Bi–Te alloy crystallized into Ge₂Bi₂Te₅, GeBi₂Te₄, GeBi₄Te₇ phase at around 300 °C according to Ge content and expelled amorphous Ge crystallized as a single phase over 400 °C. Combining these with the differential scanning calorimetry (DSC) results, we demonstrated that T_c and T_m of the Ge–Bi–Te alloy are respectively higher and lower than those of conventional Ge–Sb–Te (GST) films. All the phases, including not only various Ge–Bi–Te ternary phases but also the Ge phase crystal structure, were also confirmed with high-resolution transmission electron microscopy (HR-TEM) images and diffraction patterns. It is noted that some of the Ge₂Bi₂Te₅ grains show specific faceted planes such as {0113}, {0112}, and {0001}. Through successive analyses, we revealed the structural evolution of the Ge–Bi–Te alloy according to Ge contents and confirmed the potential of the Ge–Bi–Te alloy for phase-change random access memory (PRAM) applications.

(Some figures in this article are in colour only in the electronic version)

1. Introduction

Recently, among many other chalcogenide amorphous semiconductors, the Ge–Sb–Te (GST) system has been studied intensively for phase change memory, because of fast crystallization

and better data storage lifetime characteristics [1]. However, for achievement of high density commercial memory devices, some problems have to be solved, such as the high current pulse required for the amorphization process, because the sample must be heated to its melting point during the reset operation. Therefore, the critical issues in phase change material requirements are summarized as follows: stability at room temperature, high crystallization speed, and reduction of writing currents. Until now, many groups have tried to work out the above problems in various ways. Research into changing crystallization behavior by typical elements doping into GST, especially the $\text{Ge}_2\text{Sb}_2\text{Te}_5$ alloy [2], and decreasing the power consumption by reducing the area of the bottom-electrode contact (BEC) is being carried out. However, in the former method, there have not been any promising developments, and in the latter research, the required area has been much smaller than for the respective process node [3, 4]. Therefore, fundamental research for an alternative GST phase change material is crucial. In this paper, as a new alternative for the well known GST, a Ge–Bi–Te (GBT) alloy is now suggested because the Bi, which lies in same group as Sb but has larger atomic radius ($r_{\text{Bi}} = 0.163$ nm, $r_{\text{Sb}} = 0.153$ nm), has been regarded as increasing the crystallization speed [5]. Recently, Matsunaga *et al* [6] reported that replacement of a proportion of Sb atoms in the pseudo-binary system— $\text{GeTe-Sb}_2\text{Te}_3$ —with Bi results in faster crystallization. They explained the reason as follows; the GBT alloy in a pseudo-binary line is crystallized into a metastable simple cubic structure with $P\bar{3}m1$ space group. The structure with randomly distributed Ge, Bi, Te atoms in the 1(a) site more closely resembles an amorphous structure than the NaCl structure of GST and this assures the more rapid phase transition from the amorphous to crystalline phase and vice versa. Moreover, the Ge has been known to increase the crystallization temperature due to its strong inter-atomic bonding strength. Therefore, with the aim of checking the possibility as an alternative phase change memory material, a ternary GBT system co-sputtered by different RF power is investigated.

2. Experimental details

RF-sputtered amorphous Ge–Bi–Te (GBT) ternary chalcogenide film with a thickness of 200 nm was deposited on a $\text{SiO}_2/\text{Si}(100)$ substrate for the purpose of avoiding the substrate effects of an Si single crystal on the crystallization of GBT thin films. The deposition rate was 30 nm min^{-1} by sputtering a $\text{Ge}_{64}\text{Te}_{36}$ and Bi single target with different power in Ar ambient where the working pressure and base pressures were 1.5 and 1.2×10^{-3} mTorr, respectively. The reason why we used the Ge-rich $\text{Ge}_{64}\text{Te}_{36}$ target is such that the strong cohesive Ge inter-atomic force seems to increase the crystallization temperature of the GBT alloy. The composition was controlled by controlling the RF sputtering powers on each target which are 70 W:20 W, 70 W:30 W, and 70 W:40 W (hereafter, we called each sample GBT20, GBT30, GBT40). The constituent profile of each sample was confirmed with auger electron spectroscopy (AES) after deposition. The decrement of Ge contents with increasing Bi target sputtering power is expected. The crystallization and melting temperatures were measured by using differential scanning calorimetry (DSC). Based on the measured T_{crys} , we carried out a rapid thermal annealing (RTA) process under N_2 ambient conditions at 150, 300, and 400 °C for 1 min in order to observe the crystallization behavior and progressive change of grain shape with temperature. We conducted the x-ray diffraction (XRD) analysis for each annealed sample with fixed θ ($\theta = 3^\circ$, 2θ scan) at 30 kV, 60 mA condition using a Rigaku, D/mas-rc (12 kW). Generally, a 2θ scan is used for increasing the amount of x-ray on the thin film. We used this method in order to obtain as many diffracted peaks as possible for confirming the phase. Cross-sectional TEM specimens were prepared by the conventional method followed by ion-milling with Ar ions. Ion milling was performed using the liquid nitrogen cooling stage of a Fischione

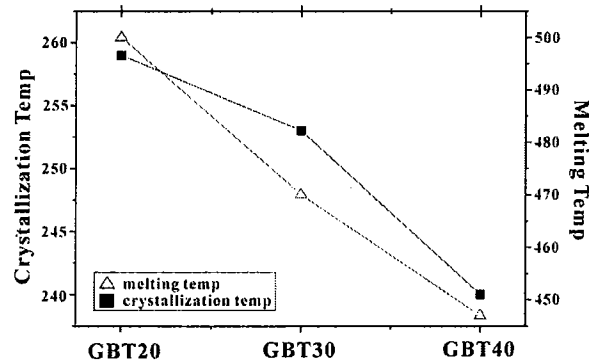


Figure 1. Crystallization and melting temperatures of GBT20, GBT30, and GBT40 samples measured by DSC.

1010 ion miller with conditions of 4 kV and 4 mA to suppress the unwanted crystallization by sample heating during the conventional Ar ion milling without cooling. Selected area electron diffraction (SAED) patterns and high-resolution transmission electron microscopy (HR-TEM) images were obtained with a JEOL JEM-2000EX operated at 200 kV and a JEM-3010 operated at 300 kV.

3. Results and discussion

According to the GBT ternary alloy phase diagram, GBT alloy is crystallized into a similar composition as the Ge–Sb–Te ternary alloy, i.e. 1:2:4, 2:2:5, 1:4:7, etc. These compositions lie along the pseudo-binary line of GeTe–Bi₂Te₃. Therefore we assume that the RF-power modulated GBT alloy crystallized into one of the stable phases in the pseudo-binary line. Firstly, we tried to confirm the constitution of each alloy. According to the AES results of as-deposited alloys, relative Ge contents of each sputtered alloy decreased from 53 at.% to 46 at.% to 43 at.% as the sputtering power on the Bi target increased. We expected the structural changes from Ge-rich type to Ge-less type alloy with deposition condition variation. However, these compositions did not seem to be satisfied with the known stoichiometric GBT alloy. In general, there exist two possible transformation mechanisms according to the composition of the amorphous state [7]. In the case of stoichiometric composition, the crystallization growth mechanism is thought to be a eutectic-interface extension, which is so-called diffusionless crystallization—growth dominant crystallization. Contrarily, in the case of non-stoichiometric composition like the above GBT alloy, due to the density gradients of atoms, the crystallization is accompanied by long range atomic diffusion as well as phase separation and follows a nucleation and growth transformation mechanism—nucleation dominant crystallization. Therefore, the activation energy shows a large value and diffusion requires a long annealing time for crystallization at high temperature close to the melting temperature. The sputtered GBT alloy seems to follow the latter transformation mechanism.

We also conducted differential scanning calorimetry (DSC) measurements. In figure 1, the crystallization and the melting temperatures of sputtered GBT alloys (GBT20, GBT30, GBT40) are shown as 259 °C, 254 °C, 240 °C and 500 °C, 470 °C, 450 °C, respectively. The T_c and T_m of pure Ge are known as 500 °C, 937 °C and those of GBT ternary alloys—GeBi₂Te₄, GeBi₄Te₇—are identified as below 200 °C, near 600 °C–587 °C, 576 °C [8, 9]. Ge inter-atomic bonding strength (263.6 kJ mol⁻¹) is higher than those of Bi (200.4 kJ mol⁻¹) and

Te (259.8 kJ mol⁻¹). In addition, Ge is well-known as one of the most effective material in increasing the T_g (the glass transition temperature), because its high coordination number (4) increases the average coordination number and bond enthalpy in the phase change material [10]. In earlier reports of excess Ge doped GST material [11], Privitera *et al* recount that after the formation of a maximum fraction crystallite of the GST phase, the crystallization rate is strongly reduced, and a further conversion of the film into a crystalline structure can occur only by increasing the annealing temperature. Therefore, Ge seems to suppress the crystallization of stoichiometric GBT alloy and this would be the reason for the high crystallization temperature. These DSC results roughly support the possibility of GBT alloy for PRAM application because the crystallization and the melting temperatures are higher and lower than those of the GST-225(151–174 °C, 632 °C) alloy which is known as the most promising material for PRAM. It is thought that high crystallization temperature guarantees the stability at room temperature, and low melting temperature ensures a reduction in the writing current during the reset operation of PRAM. Generally, contradiction between speed and stability of phase change material is commonly solved by sacrificing speed so as to ascertain the stability. Compared with conventional GST properties, we expected both the improvement of crystallization speed by Bi and advancement of stability by Ge. However, Ge has more effect on the properties of GBT alloy than Bi. With regard to the crystallization speed of sputtered GBT alloy, those of GBT20, GBT30, and GBT40 alloys are slower than that of GST. Because, $\Delta T = T_m - T_x$ values of all GBT alloys which are proportional to the driving force for crystallization depicted as $-\Delta G_v = \Delta H_f \Delta T / T_m$ are smaller than that of GST. Consequently, the sputtered GBT alloy attained more stability than preexisting GST with increased crystallization temperature and lowered melting temperature. It is thought that we have made a good compromise between the two counter factors.

In figure 2, we show XRD results of each sample. Figure 2(a) represents the series XRD features of GBT20 samples which are for the as-deposited one as well as the annealed one at 150 °C and 300 °C for 1 min. The GBT20 alloy maintains the amorphous state until 150 °C. At 300 °C, the observed crystalline peaks were confirmed as Ge₂Bi₂Te₅ phase. Commonly, GBT ternary alloy structure can be inferred from the GeTe–Bi₂Te₃ pseudo-binary system and all the intermediate stable structures are explained by the nGeTe–mBi₂Te₃ form [12]. Therefore, intermediate structures can be divided into two parts, the GeTe-rich region and the Bi₂Te₃-rich region. Compositions of 5:2:8, 4:2:7, 3:2:6, 2:2:5, 1:2:4 can be shown in the former region and 1:4:7, 1:6:10, 1:8:13 in the latter region. Among them, the well-known stable composition structures are Ge₂Bi₂Te₅ ($n = 2, m = 1$), GeBi₂Te₄ ($n = 1, m = 1$), GeBi₄Te₇ ($n = 1, m = 2$) [13]. The Ge₂Bi₂Te₅ unit cell ($a = 0.4286$ nm, $c = 1.7394$ nm, space group is $P\bar{3}m1$) consists of one nine-layer packet—TeMeTeMeTeTeMeTeMe—(Me is mixed Bi/Ge layer) with $N = 9$, where N is the number of atomic layers along the c -axis per unit cell. Similarly, the GeBi₂Te₄ unit cell ($a = 0.4322$ nm, $c = 4.172$ nm, space group is $R\bar{3}m$) consists of three seven-layer packets—TeMeTeMeTeTeMe—(Me is mixed Bi/Ge layer) with $N = 21$. In these two phases, the structures are very similar, e.g. the (0009) inter-planar spacing of Ge₂Bi₂Te₅, 0.1983 nm, is akin to the GeBi₂Te₄(00021) spacing, 0.1965 nm. Thus, the Bragg diffraction will occur at a similar angle. In figure 2(c), simulated XRD patterns of GeBi₄Te₇, GeBi₂Te₄, and Ge₂Bi₂Te₅ structures, four of the most intensive diffracted peak positions of GeBi₂Te₄ and Ge₂Bi₂Te₅ are very alike (#1—28.22°, 28.55°, #2—38.85°, 39.47°, #3—41.76°, 41.71°, #4—51.17°, 51.68°). Moreover, similar polytypical phases formed by the weak van der Waals forces usually show very small energy differences that can cause various crystallographic transitions [14]. Therefore, GeBi₂Te₄ and Ge₂Bi₂Te₅ phases are seen to co-exist at 300 °C for the annealed GBT20 alloy. According to Karpinsky *et al* [15], significant changes in the number of N layers per unit cell are observed with increasing excess of Ge

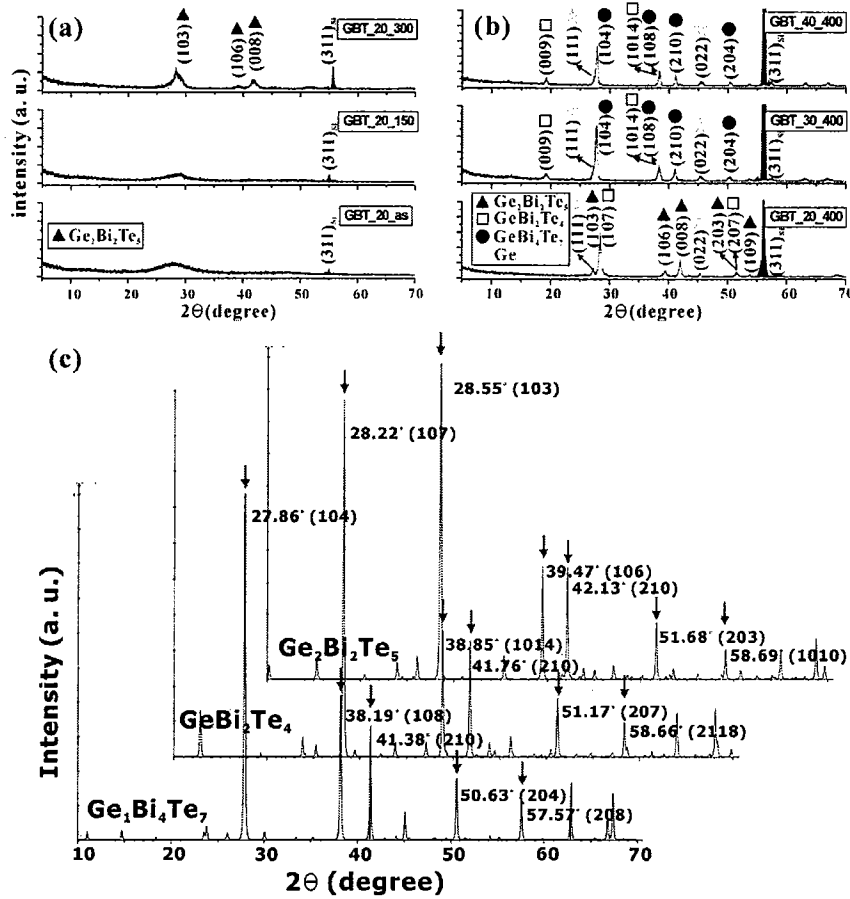


Figure 2. X-ray diffraction data of (a) GBT20 samples at as-deposited state, 150 °C, 300 °C and (b) 400 °C annealed GBT20, GBT30, and GBT40. (c) Simulated XRD patterns of Ge₂Bi₂Te₅, GeBi₂Te₄, and GeBi₄Te₇ alloy.

for the alloys of GeBi₂Te₄ + Ge and GeBi₄Te₇ + Ge. The former changes to Ge₂Bi₂Te₅ and the latter transforms to GeBi₂Te₄ and Ge₂Bi₂Te₅. Conversely, this means that GBT20, which shows the largest Ge content among sputtered samples, firstly crystallize into the Ge₂Bi₂Te₅ (23 at.% Ge) phase. As temperature increases, excess Ge come out and crystallizes as a single phase and the remaining Ge₂Bi₂Te₅ transforms into GeBi₂Te₄ (14 at.% Ge). GBT30, GBT40 with relatively less Ge content crystallize into the GeBi₄Te₇ (8.3 at.% Ge) phase. XRD data of 400 °C annealed GBT30 and GBT40 in figure 2(b) show that GeBi₂Te₄ and GeBi₄Te₇ exist together. It is known that the phase separation during crystallization must be accompanied by slow diffusion of atomic species, which limits the crystallization speed and is the main cause of deterioration of memory devices [16–19]. However, Liu *et al* [20] reported that phase separation increased the resistance due to current carrier scattering by the crystalline boundary. In this experiment, we did not find significant worsening in properties of the films caused by phase separation.

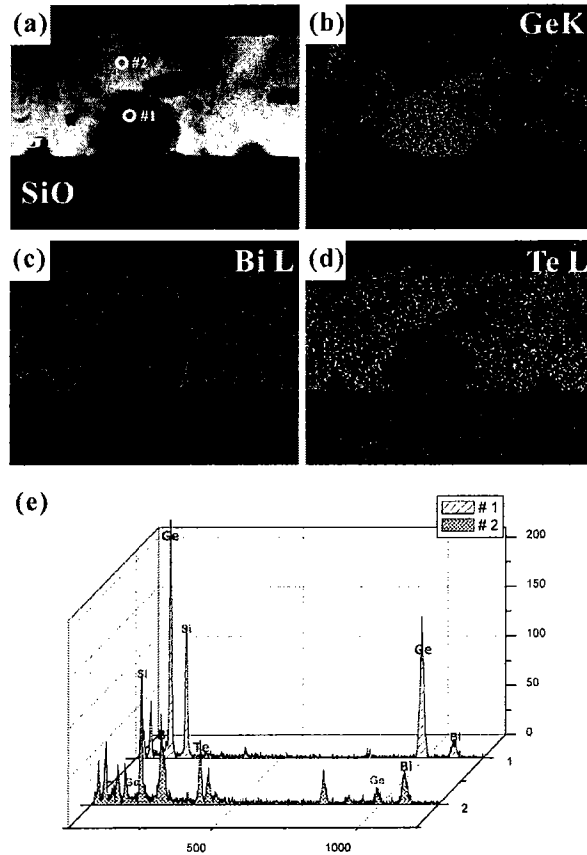


Figure 3. (a) High angle annular dark-field image of 400 °C annealed GBT20 sample and (b)–(d) corresponding energy dispersive spectroscopy (EDS) elemental mapping images. (e) EDS data of the neighboring region in thin films marked #1 and #2 in figure 3(a).

The existence of the Ge phase was confirmed with energy dispersive spectroscopy (EDS) experiments with the 400 °C annealed GBT20 sample. Mapping results of each element (Ge, Bi, Te) are presented in figure 3. The nearest two grains show a different composition ratio, one of which is Ge dominant (#1) and the other is Bi–Te dominant (#2). This result supports the result that excess of Ge atoms diffuse out from the GeTe-rich type GBT grains like GeBi_2Te_4 or $\text{Ge}_2\text{Bi}_2\text{Te}_5$ and crystallize over 400 °C. Thus this phenomenon affects the crystallization and melting temperature of sputtered GBT alloy. We think that more detailed research of the Ge phase effect on the GBT alloy properties will be needed. In figure 4, bright-field transmission electron microscopy (BF-TEM) images and corresponding diffraction patterns of annealed GBT20 sample are shown. Overall results such as amorphous phase preservation up to 150 °C, the co-existence of GBT ternary crystallite and residual amorphous Ge phase over 300 °C (diffraction spots with halo rings), and the appearance of the crystalline Ge phase at 400 °C all coincide with XRD data. In figures 4(c) and (d), the size of crystalline grains in

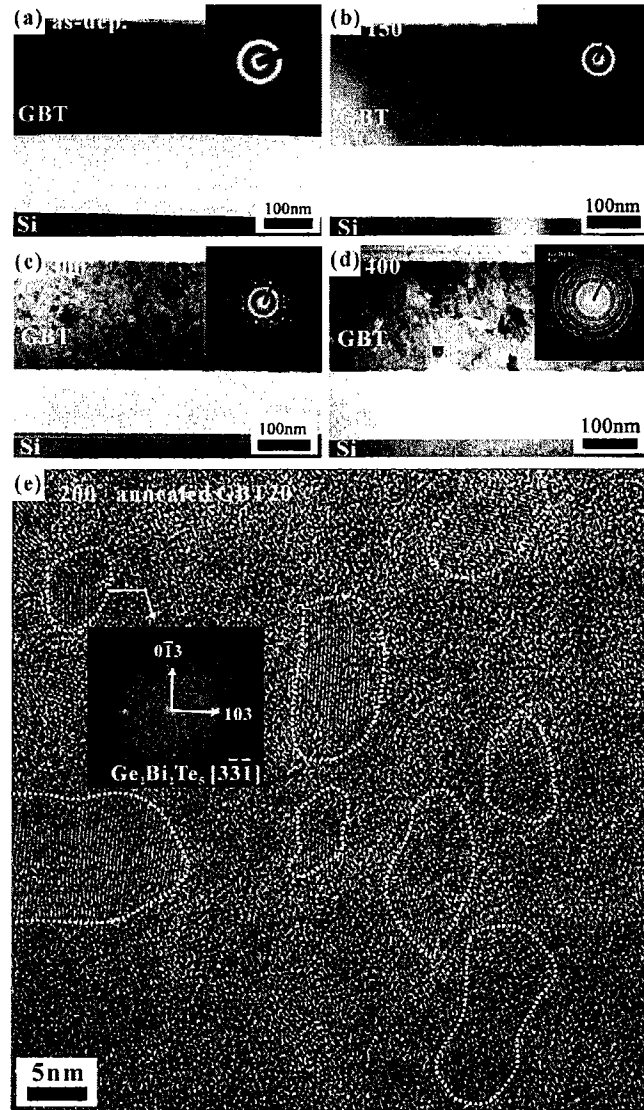


Figure 4. BF-TEM images and corresponding diffraction patterns of the GBT20 sample. (a) As-deposited state, annealed at (b) 150 °C (c) 300 °C, and (d) 400 °C for 1 min are shown. (e) HR-TEM image of the 200 °C annealed GBT20 sample which represents competitive small nuclei formation.

300 °C and 400 °C annealed samples varies from several nm to 100 nm. Furthermore, the high resolution image of 200 °C annealed GBT20 in figure 4(e) represents crystallization initiated by randomly formed small nuclei. From these results, we deduced that the crystallization follows the nucleation-growth mechanism—crystallization proceeds mainly via the generation of small nuclei which are sufficiently large and grow competitively over 400 °C.

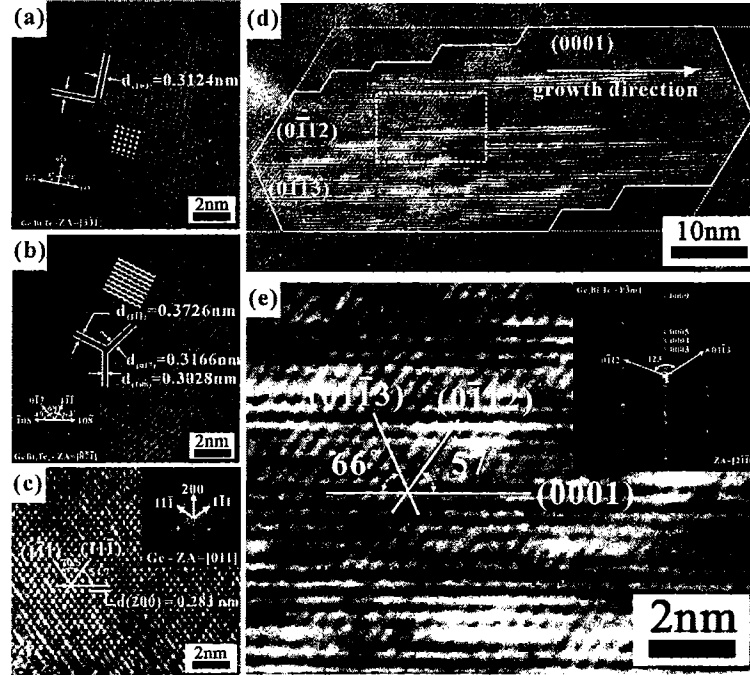


Figure 5. HR-TEM images of $\text{Ge}_2\text{Bi}_2\text{Te}_5$, GeBi_2Te_4 , Ge phase observed at 400°C for the annealed sample viewed along (a) $\text{Ge}_2\text{Bi}_2\text{Te}_5$ - $[\bar{3}\bar{3}\bar{1}]$, (b) GeBi_2Te_4 - $[\bar{8}\bar{7}\bar{1}]$, (c) Ge- $[011]$ directions are shown with simulated image. (d) HR-TEM image of $\langle 2110 \rangle$ zone-axis $\text{Ge}_2\text{Bi}_2\text{Te}_5$ phase is shown in which we verify the atomic layer structure and inter-planar angles. (e) Enlarged image of rectangular area in figure 5(d).

In figure 5, we show the HR-TEM images of 400°C annealed samples in order to unravel the accurate structure and phase. We superimposed the image simulated with NCEM (National Center for Electron Microscopy) software with adequate defocus and thickness conditions on each image. As mentioned above, the GBT ternary alloy structures generally show the layered structure in the rhombohedral Bravais lattice. Therefore, in order to investigate the atomic layer sequence of a rhombohedral structured alloy, one should view the structure along the $\langle 2110 \rangle$ or $\langle 0110 \rangle$ direction. However, including the a -axis direction, $\langle 2110 \rangle$, GBT ternary structures are observed along the high index zone axis— $[\bar{3}\bar{3}\bar{1}]$, $[\bar{8}\bar{7}\bar{1}]$. Actually, the atomic arrangement along viewing directions in figures 5(a) and (b) is very symmetrical to get a high resolution image. In figure 5(c), the Ge phase observed in 400°C annealed alloy is shown. Figure 5(d) depicts several tens of nm-sized specific grains annealed at 300°C , which are viewed along the $\langle 2110 \rangle$ direction. The growth direction of the grain is $\langle 0001 \rangle$. Note that specific faceted planes like $\{0112\}$, $\{0113\}$, and $\{0001\}$ are observed. The appearance of characteristic faceted planes have been reported before in GST-225 alloy [21]. According to the broken bond model [22], only two planes having the lowest surface energy— $\{0001\}$, $\{0112\}$ —can remain, and the highest surface energy plane among them— $\{0113\}$ —will vanish as the crystallization goes on. The expected grain shape is represented by a dotted line.

4. Conclusion

We conducted the compositional analysis and structural characterization of series annealed Ge–Bi–Te ternary phase change material. Through AES analysis, we confirmed that the elemental composition of as-deposited film showed a non-stoichiometric constitution. XRD results of the 400 °C annealed sample showed the existence of various Ge–Bi–Te ternary phases along the Bi₂Te₃–GeTe pseudo-binary line. As the relative amount of Ge decreases from GBT20 (53 at.% Ge) to GBT30 (46 at.% Ge) to GBT40 (43 at.% Ge), ternary alloy composition varies from Ge₂Bi₂Te₅ to GeBi₂Te₄ to GeBi₄Te₇ with excess of Ge phase. Moreover, EDS results manifested the reason for the appearance of the Bi–Te-rich phase with increasing annealing temperature; the formation of the GeTe-rich ternary alloy was less favored than the separation of the Ge phase and the Bi–Te-rich phase. Through TEM analysis, we showed the initiation of crystallite formation and that the crystallization of GBT alloy occurred mainly by a nucleation-growth mechanism. In addition, every phase existing in the GBT alloy was confirmed by HR-TEM images viewed along various zone axes. Furthermore, from the specific facet planes, we predicted the grain growth direction—[0001]—and the final stable structure with energetically favorable planes—{0001}, {0112} planes.

Acknowledgments

This work was supported by Samsung Electronics and the Korean Ministry of Commerce, Industry, and Energy (MOCIE) under the National Research Project of Phase-Change Random Access Memory Development.

References

- [1] Gill M, Lowrey T and Park J 2002 *IEEE ISSCC Dig. Tech. Pap.* p 202
- [2] Matsuzaki N, Kurotsuchi K, Matsui Y, Tonomura O, Yamamoto N, Fujisaki Y, Kitai N, Takemura R, Osada K, Hanazawa S, Moriya H, Iwasaki T, Kawahara T, Takaura N, Terao M, Matsuoka M and Moniwa M 2005 *IEDM Technical Digest* p 738
- [3] Ahn S J, Hwang Y N, Song Y J, Lee S H, Lee S Y and Park J H 2005 *Symp VLSI Tech, Tech Dig* pp 98–9
- [4] Cho S L, Yi J H, Ha Y H, Kuh B J, Lee C M and Park J H 2005 *Symp. VLSI Tech, Tech. Dig.* pp 96–7
- [5] Wang K, Wamwangi D, Ziegler S, Sfeimer C and Wuttig M 2004 *J. Appl. Phys.* **96** 5557–62
- [6] Matsunaga T and Yamada N 2004 *Japan. J. Appl. Phys.* **43** 4704–12
- [7] Situ H, Wang Z T and Jung A L 1989 *J. Non-Cryst. Solids* **113** 88–93
- [8] Chambouleyron I, Fajardo F and Janatta A R 2002 *J. Non-Cryst. Solids* **299** 143–7
- [9] Skoropanov A S, Walowski B L, Samal G L, Alfer S A and Wetscher A A 1987 *Z. Phys. Chem.* **268** 97
- [10] Lankhorst M H R 2002 *J. Non-Cryst. Solids* **297** 210–9
- [11] Privitera S, Rimini E, Bongiorno C, Zonca R, Pirovano A and Bez R 2003 *J. Appl. Phys.* **94** 4409–13
- [12] Shelimova L E, Carpinski O G, Konstantinov P P, Avilov E S, Kretova M A and Zemskov V S 2004 *Inorg. Mater.* **405** 451–60
- [13] Shelimova L E, Konstantinov P P, Karpinsky O G, Avilov E S, Kretova M A and Zemskov V S 2001 *J. Alloys Compounds* **329** 50–62
- [14] Kuznetsova L A, Kuznetsov V L and Rowe D M 2000 *J. Phys. Chem. Solids* **61** 1269–74
- [15] Karpinsky O G, Shelimova L E, Kretova M A and Fleurial J-P 1997 *J. Alloys Compounds* **265** 170–5
- [16] Nakayama K, Kojima K, Hayakawa F, Imai Y, Kitagawa A and Suzuki M 2000 *Japan. J. Appl. Phys.* **39** 6157–61
- [17] Privitera S, Rimini E, Bongiorno C, Zonca R, Pirovano A and Bez R 2003 *J. Appl. Phys.* **94** 4409–13
- [18] Coombs J H, Jongenelis A P J M, van Es-Spiekman W and Jacobs B A 1995 *J. Appl. Phys.* **78** 4918–28
- [19] Chem M, Rubin K A and Barton R W 1986 *Appl. Phys. Lett.* **49** 502–4
- [20] Liu B, Song Z, Feng S and Chen B 2005 *Mater. Sci. Eng. B* **119** 125–30
- [21] Park Y J, Lee J Y and Kim Y T 2006 *Appl. Phys. Lett.* **88** 201905–7
- [22] Porter D A and Easterling K E 1992 *Phase Transformations in Metals and Alloys* (London: Chapman and Hall)



Effect of deposition temperature on the structural and thermoelectric properties of bismuth telluride thin films grown by co-sputtering

Dong-Ho Kim ^{a,*}, Eungsun Byon ^a, Gun-Hwan Lee ^a, Sunglae Cho ^b

^a Surface Technology Research Center, Korea Institute of Machinery and Materials (KIMM), Changwon, Kyungnam 641-010, South Korea

^b Department of Physics, University of Ulsan, Ulsan 680-749, South Korea

Received 13 July 2005; received in revised form 15 December 2005; accepted 22 December 2005

Available online 8 February 2006

Abstract

Thermoelectric bismuth telluride thin films were prepared on SiO₂/Si substrates by radio-frequency (RF) magnetron sputtering. Co-sputtering method with Bi and Te targets was adopted to control films' composition. Bi_xTe_y thin films were elaborated at various deposition temperatures with fixed RF powers, which yielded the stoichiometric Bi₂Te₃ film deposition without intentional substrate heating. The effects of deposition temperature on surface morphology, crystallinity and electrical transport properties were investigated. Hexagonal crystallites were clearly visible at the surface of films deposited above 290 °C. Change of dominant phase from rhombohedral Bi₂Te₃ to hexagonal BiTe was confirmed with X-ray diffraction analyses. Seebeck coefficients of all samples have negative value, indicating the prepared Bi_xTe_y films are n-type conduction. Optimum of Seebeck coefficient and power factor were obtained at the deposition temperature of 225 °C (about −55 μV/K and 3 × 10^{−4} W/K²·m, respectively). Deterioration of thermoelectric properties at higher temperature could be explained with Te deficiency and resultant BiTe phase evolution due to the evaporation of Te elements from the film surface.

© 2006 Elsevier B.V. All rights reserved.

PACS: 71.55.Ak; 73.50.Lw; 73.50.-h; 81.15.Cd

Keywords: Bismuth telluride; Thermoelectric thin film; Electrical transport properties; Sputtering

1. Introduction

Recent achievements of high efficient thermoelectricity in semiconductor nanostructures have brought much attention on thermoelectric devices [1–4]. Application of thermoelectric micro-cooling device is very promising for thermal management of microelectronics and optoelectronics.

Bismuth telluride (Bi₂Te₃) and its solid solutions are well known thermoelectric materials for near-room temperature applications. They are narrow-bandgap semiconductors with rhombohedral layered crystal structure. Preparation of these chalcogenide thermoelectric materials in thin film form is highly required to fabricate an active micro-cooling device in chip level. Bismuth telluride thin films have been elaborated by a variety of deposition techniques, such as evaporation [5–8],

pulsed laser deposition [9,10], sputtering [11], and electrochemical deposition [12]. Even though high quality epitaxial films could be obtained by metal organic chemical vapor deposition (MOCVD) [13,14] and molecular beam epitaxy (MBE) [15,16], preparation of thermoelectric films by more conventional deposition technique is highly requested in related industry. In this work, bismuth telluride films were prepared by RF magnetron sputtering process, which is industrially friendly. It is well known that the thermoelectric properties of Bi₂Te₃ films are strongly dependent on the stoichiometry. Usually in vacuum process, however, the difference in vapor pressures of Bi and Te elements leads to the deviation from the stoichiometric composition due to the re-evaporation of Te element from a deposited film.

In this study, bismuth telluride films were elaborated by co-sputtering of constituent elements in order to control films' composition. The effects of deposition temperature on structural properties of Bi_xTe_y films were investigated. Thermoelectric

* Corresponding author. Tel.: +82 55 280 3557; fax: +82 55 280 3590.

E-mail address: dhkim2@kmail.kimm.re.kr (D.-H. Kim).

properties (electrical transport properties, Seebeck coefficient and power factor) of the films were also examined.

2. Experimental details

Bismuth telluride thin films were prepared by using a RF magnetron sputtering system, described in our previous work [17]. Schematic diagram of experimental setup is shown in Fig. 1. High purity (99.999%) bismuth and tellurium targets with a diameter of 2 in. were used as the source materials and they were connected to each RF power supplier. Films were deposited on silicon (001) substrates with thermally grown oxide overlayer (300 nm) for the purpose of electrical and thermal isolation. The distance between the targets and the substrate was kept at 50 mm and substrates were rotated at 100 rpm for uniform film deposition. The base pressure of the deposition chamber was below 1.5×10^{-4} Pa and the working pressure was set at 8×10^{-2} Pa, flowing 3 sccm of Ar as the sputtering gas.

Prior to depositing films at various substrate temperatures, we have chosen RF powers for each target. At a fixed power (20 W) for Bi target, bismuth telluride films were prepared with varying the power for Te target. In this step, depositions were carried out without intentional substrate heating. Energy dispersive X-ray spectroscopy (EDS) with a scanning electron microscope (SEM, JEOL JSM 5800) was used to measure the composition. Atomic percent of Te in a film was determined by averaging the values measured at least 5 points on the film's surface. As shown in Fig. 2, Te content in deposited films has a linear dependence on its RF power in range of 25–45 W. Stoichiometric Bi_2Te_3 film could be obtained with Te power of ~ 43 W. All the specimens in this work were prepared with these RF powers (Bi=20 W, Te=43 W). The substrate temperature was varied from 27 to 320 °C which was controlled with a resistive graphite heater, lying below the substrate holder. Depositions were carried out during 10 min. Step height of a deposited layer was measured with a surface profiler (Tencor P-11). Thickness of films deposited in this process condition was around 400 nm in average, while their roughness increased more than 100 nm at elevated deposition temperature.

Surface morphology of bismuth telluride films was observed with a field emission SEM (JEOL, JSM-6700 F) operating at 5 kV and crystallinity was characterized with a X-ray diffraction system (Philips, X'pert APD) in the conventional $\theta-2\theta$ mode

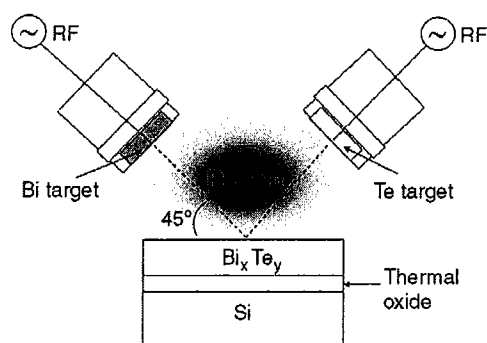


Fig. 1. Schematics of experimental setup for co-sputtering.

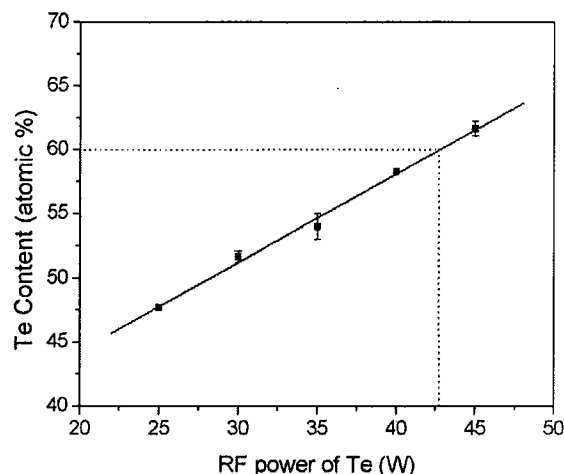


Fig. 2. Te contents in deposited films as a function of RF power of Te target.

by use of the $\text{Cu K}\alpha_1$ line for the X-ray source. Electrical transport properties were measured with the van der Pauw method of measuring the Hall coefficient. Seebeck coefficient (or thermopower) of a film was determined with a temperature gradient method.

3. Results and discussion

3.1. Surface morphology and crystallinity

Film deposited at room temperature (not shown here) has a shiny and very smooth surface and there is no crystalline phase on surface. Polycrystalline films were obtained at elevated temperatures. Since the deposition was performed on amorphous oxide layer, epitaxial film growth was not possible. Effect of the substrate temperature on morphology of polycrystalline films is clearly evident in Fig. 3. With the increase of the temperature, surface diffusion and agglomeration of adatoms were enhanced. Film deposited at 165 °C is composed of grains with size of ~ 100 –200 nm. At higher substrate temperature, larger grains were generated due to coalescence of small grains and diffusion of adatoms. Grain boundaries and intervening voids are clearly visible in Fig. 3 (d). Above 290 °C, however, a quite different type of grain structure was observed in our bismuth telluride film. Hexagonal crystallites as large as ~ 1 μm were formed during the deposition, as shown in Fig. 3 (e) and (f).

X-ray diffraction patterns of bismuth telluride thin films are shown in Fig. 4. From the comparison with a powder diffraction file (JCPDS card 15-863), it was seen that the patterns of the films deposited lower than 290 °C can be attributed to the rhombohedral Bi_2Te_3 structure. It is observed that the films deposited at 225 and 260 °C have the preferred orientation of the (015) lattice plane. Above 290 °C, however, the peak positions and their intensities were obviously changed. Even though the strongest peak of (015) plane in Bi_2Te_3 phase overlaps in position with the peak of (104) plane in BiTe phase (JCPDS card 44-667), it is clear that the peaks of the (005) and (0012) planes in the BiTe phase arose at high deposition temperatures. It reveals that the hexagonal BiTe phase became dominant in

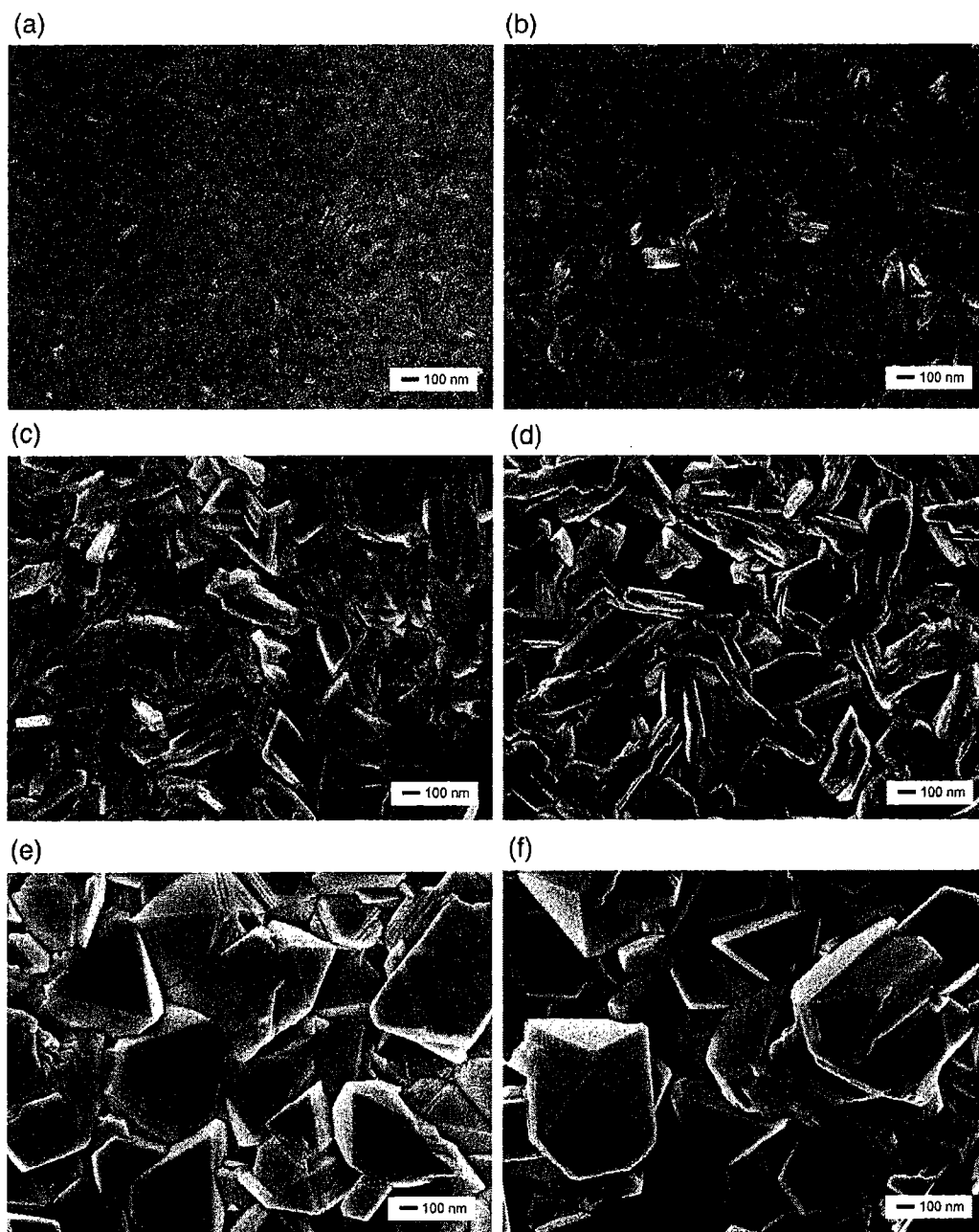


Fig. 3. FESEM images of bismuth telluride thin films deposited at (a) 100 °C, (b) 165 °C, (c) 225 °C, (d) 260 °C, (e) 290 °C, and (f) 320 °C.

polycrystalline Bi_xTe_y thin films deposited at these high temperatures. It is consistent with the occurrence of hexagonal crystallite in SEM observation. The change of dominant phase from Bi_2Te_3 to BiTe is considered to come from non-stoichiometry in films deposited at high substrate temperature. Since the relative amounts of Bi_2Te_3 and BiTe phase in the deposited films could not be determined in our XRD analysis, the compositions of the films were examined with EDS. It was found that films deposited at high temperature (≥ 290 °C) are Te deficient (Fig. 5). Considering the vapor pressures of constituent elements [11], we concluded that in our sputtering condition (8×10^{-2} Pa) tellurium elements which did not make a compound with Bi atoms were evaporated around 300 °C. Therefore,

it is necessary to adjust the target power for the exact stoichiometry above this temperature.

4. Thermoelectric properties

Along with the structural characteristics, electrical transport properties of bismuth telluride thin films were also strongly affected by the deposition temperature. Hall effect measurements were carried out at room temperature and the measured data are plotted in Fig. 6. With increasing the substrate temperature, the carrier concentration of thin film was decreased due to the reduction of defects in polycrystal. And the mobility of charge carriers was increased according to the grain growth. The

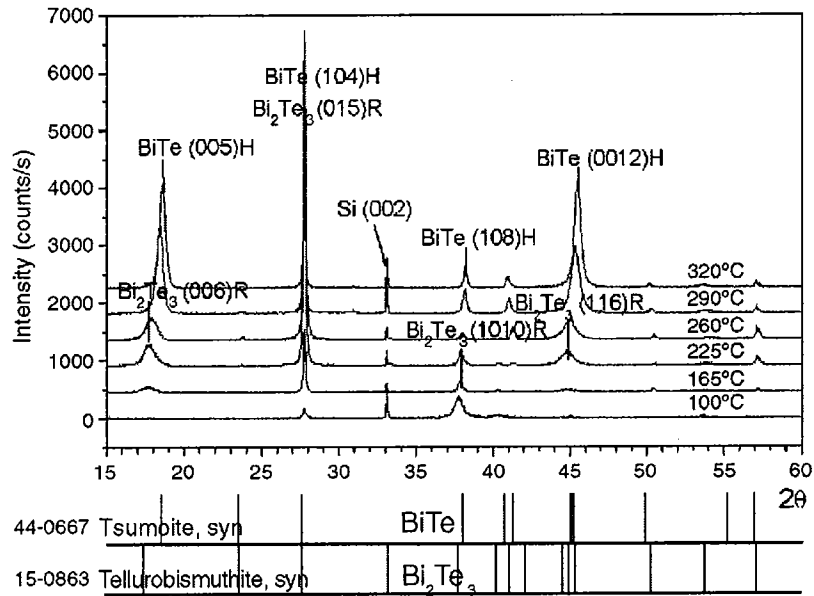


Fig. 4. X-ray diffraction patterns of bismuth telluride films deposited at various substrate temperatures.

mobility has a maximum value of $\sim 45 \text{ cm}^2/\text{V}\cdot\text{s}$ at 225°C . This mobility is an order of magnitude lower than those obtained on bulk alloys [18] and epitaxial films grown by MBE [15]. It is clearly due to the polycrystalline nature of sputter deposited films. The corresponding minimum value of carrier concentration is $\sim 1.3 \times 10^{20}/\text{cm}^3$. Above this temperature, the mobility decreased with increasing carrier concentration, as expected in semiconductor materials. This kind of variation in electrical characteristics was also reported in Bi_2Te_3 films grown by co-evaporation [7] and MOCVD [14]. Abrupt increase of carrier concentration at 290°C is thought to result from the Te deficiency. This deviation from stoichiometry for Bi_2Te_3 induced the increase of carrier concentration with a sacrifice of mobility, i.e. the charge carrier encounters lots of the defect scattering centers. Resistivity (ρ) of the films was found to be decreased with increasing the substrate temperature. Films deposited above

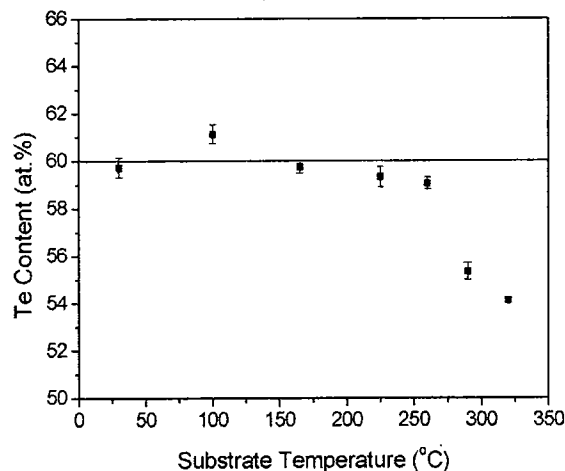


Fig. 5. Te contents in bismuth telluride films as a function of deposition temperature.

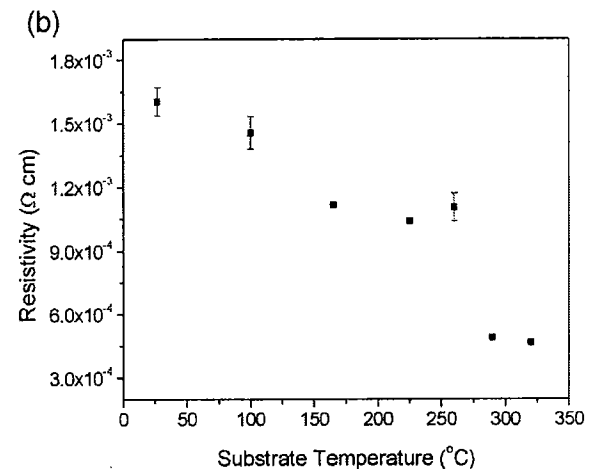
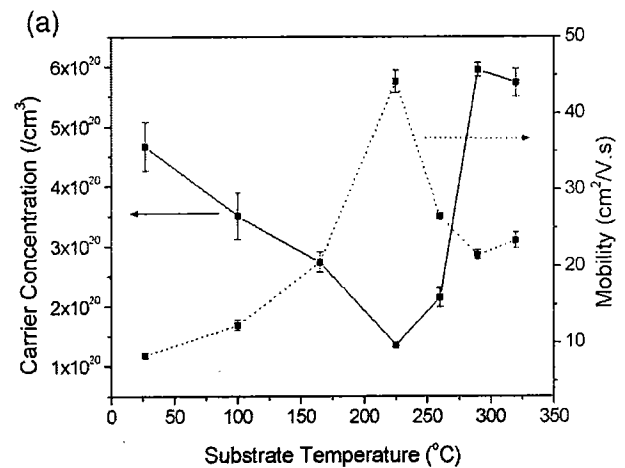


Fig. 6. Electrical transport properties of bismuth telluride films as a function of the deposition temperature.

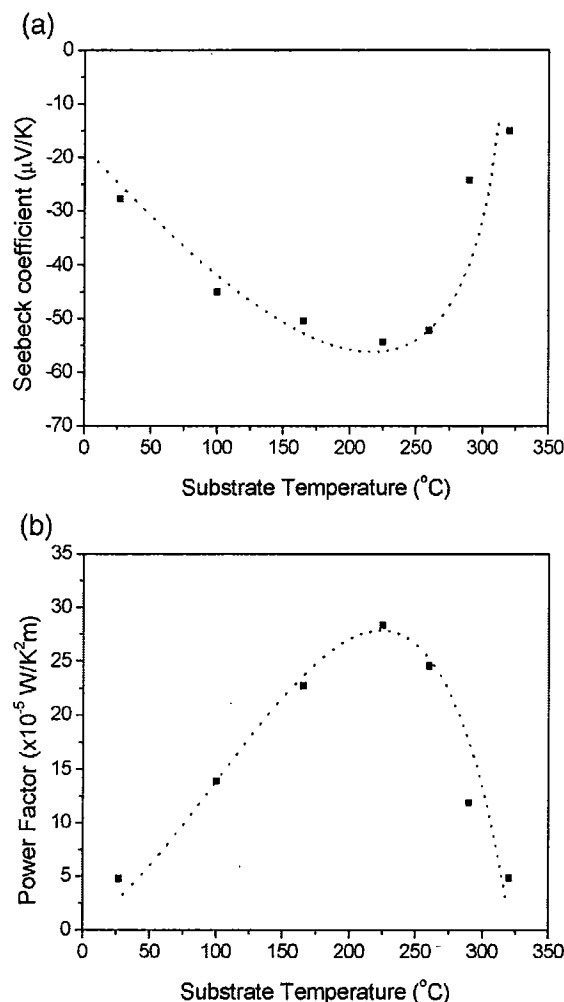


Fig. 7. Seebeck coefficients and power factors of bismuth telluride films as a function of the deposition temperature (lines only as guide to eye).

290 $^{\circ}\text{C}$ have fairly small values of electrical resistivity. Large electrical conductivity is favorable in view of thermoelectric efficiency. However, these films are expected to have relatively small values of Seebeck coefficient since BiTe phase is dominant (as noted in previous section). It is well known that the stoichiometric Bi_2Te_3 film has a high crystallinity, high electron mobility, and high thermopower [15]. In this work nearly stoichiometric films could be obtained at lower deposition temperatures; nevertheless, our sputter deposited films have polycrystalline nature and their thermoelectric properties are expected to be restricted.

Seebeck coefficient of a thin film was determined from the plot of the measured Seebeck voltage versus the temperature difference across the specimen ($S = \Delta V / \Delta T$). Fig. 7 shows the influence of the substrate temperature on Seebeck coefficients and power factors (S^2/ρ) of films. All the samples have negative values of Seebeck coefficient, indicating our Bi_xTe_y thin films are n-type thermoelectric. Around 225 $^{\circ}\text{C}$, the absolute value of Seebeck coefficient has its maximum of $\sim 55 \mu\text{V/K}$, which is about one fourth of those obtained on Bi_2Te_3 single

crystals. It is considered that large density of defects in polycrystalline films and resultant small mobility caused the difference. Optimum of power factor also exists at 225 $^{\circ}\text{C}$, since the film deposited at this temperature has the lowest resistivity and the highest Seebeck coefficient. The maximum value of power factor is $\sim 3 \times 10^{-4} \text{ W/K}^2\text{m}$.

As expected, thermopower (or Seebeck coefficient) and power factor of the films became worse at further higher temperatures. It can be explained with the result that stoichiometric Bi_2Te_3 films could not be obtained at these process conditions (RF powers of Bi and Te, deposition temperature). Even though films deposited at these temperatures have small values of electrical resistivity, these films are non-stoichiometric for Bi_2Te_3 and mainly composed of BiTe phase.

5. Conclusion

Thermoelectric bismuth telluride thin films were grown on SiO_2/Si substrates using the RF magnetron co-sputtering method. The influence of deposition temperature on the structural and thermoelectric properties was investigated. Stoichiometric Bi_2Te_3 thin films were obtained when deposition was performed at substrate temperature below 290 $^{\circ}\text{C}$. Above this temperature evolution of hexagonal crystallites and deviation from the stoichiometry (Bi:Te=2:3) were identified. X-ray diffraction analyses confirmed the change of dominant phase from rhombohedral Bi_2Te_3 to hexagonal BiTe. Thermoelectric properties were found to be strongly dependent on the deposition temperature. Bi_2Te_3 film deposited at 225 $^{\circ}\text{C}$ has largest mobility and smallest carrier concentration. Optimum of thermoelectric properties was also obtained at this temperature. Maximum values of $|S|$ and power factor of our n-type thermoelectric thin films are $\sim 55 \mu\text{V/K}$ and $\sim 3 \times 10^{-4} \text{ W/K}^2\text{m}$, respectively. Even though these values are quite smaller than those of bulk and epitaxial films, improvement of the thermoelectric properties is expected to be achieved with stoichiometry control at the elevated temperature and post-annealing treatments.

Acknowledgements

This research is implemented as a part of the project "Technology Development of Advanced Cooling System" managed by Korea Research Council for Industrial Science and Technology. The authors gratefully appreciate the support.

References

- [1] C.B. Vining, Nature 413 (2001) 577.
- [2] G. Chen, M.S. Dresselhaus, G. Dresselhaus, J.-P. Fleurial, T. Caillat, Int. Mater. Rev. 48 (2003) 1.
- [3] B.C. Sales, Science 295 (2002) 1248.
- [4] A. Majumdar, Science 303 (2004) 777.
- [5] F. Völklein, V. Baier, U. Dillner, E. Kessler, Thin Solid Films 187 (1990) 253.
- [6] K.-W. Cho, I.-H. Kim, Mater. Lett. 59 (2005) 966.
- [7] H. Zou, D.M. Rowe, G. Min, J. Cryst. Growth 222 (2001) 82.
- [8] J. Dheepa, R. Sathyamoorthy, S. Velumani, A. Subbarayan, K. Natarajan, P.J. Sebastian, Sol. Energy Mater. Sol. Cells 81 (2004) 305.
- [9] A. Dauscher, A. Thomy, H. Scherrer, Thin Solid Films 280 (1996) 61.

- [10] R.S. Makala, K. Jagannadham, B.C. Sales, *J. Appl. Phys.* 94 (2003) 3907.
- [11] H. Noro, K. Sato, H. Kagechika, *J. Appl. Phys.* 73 (1993) 1252.
- [12] B.Y. Yoo, C.-K. Huang, J.R. Lim, J. Herman, M.A. Ryan, J.-P. Fleurial, N.V. Myung, *Electrochim. Acta* 50 (2005) 4371.
- [13] A. Boulouz, S. Chakraborty, A. Giani, F.P. Delannoy, A. Boyer, J. Schumann, *J. Appl. Phys.* 89 (2001) 5009.
- [14] A. Giani, A. Boulouz, F.P. Delannoy, A. Foucaran, A. Boyer, *Mater. Sci. Eng., B, Solid-State Mater. Adv. Technol.* 64 (1999) 19.
- [15] S. Cho, Y. Kim, A. DiVenere, G.K. Wong, J.B. Ketterson, R. Meyer, *Appl. Phys. Lett.* 75 (1999) 1401.
- [16] Y. Kim, S. Cho, A. DiVenere, G.K. Wong, J.B. Ketterson, *Phys. Rev., B* 63 (2001) 155306.
- [17] D.-H. Kim, S.-H. Lee, J.-K. Kim, G.-H. Lee, *Appl. Surf. Sci.*, in press.
- [18] D.-H. Kim, T. Mitani, *J. Alloys Compd.* 399 (2005) 14.